

ARTICLE OPEN



Unraveling the strong covariability of tropical cyclone activity between the Bay of Bengal and the South China Sea

Zeming Wu¹, Chundi Hu^{1,2,3}, Lifei Lin^{4,5}, Weizhen Chen^{4,5}, Lixuan Huang^{4,5}, Zijian Lin¹ and Song Yang^{2,4,5}

Herein, we report a strong in-phase covariability of tropical cyclone (TC) activity between the Bay of Bengal (BOB) and the South China Sea (SCS) during October–December of 1979–2019, and which is also the dominant mode of BOB–SCS TC activity, accounting for 35% of the total variances in TC track density. This inter-basin TC covariance is closely linked to the anomalies of tropical sea surface temperature, appearing as the intrinsic Indo-Pacific Tripole mode, which significantly affects the atmospheric circulations overlying the BOB–SCS. Interestingly, this mechanism works via modulating the local TC genesis frequency in the BOB–SCS. However, in terms of the migrated TCs among them, the Indo-Pacific Tripole mainly regulates their genesis location but not their frequency. More importantly, such inter-basin TC covariability still exists significantly even when the TC track data migrating from the SCS into the BOB are excluded. After all, only 19 TCs during the 41 years (1979–2019) are observed to migrate from the SCS to the BOB, which can only contribute slightly to increasing the covariability of BOB–SCS TC-track activity, but do not play a dominant role. Further, the numerical simulations suggest that although both the Indian and Pacific Oceans contribute to the atmospheric anomalies that affect the BOB–SCS TC activity, the Pacific-effect is twice as important.

npj Climate and Atmospheric Science (2023)6:180; <https://doi.org/10.1038/s41612-023-00506-z>

INTRODUCTION

Although the Bay of Bengal (BOB) is not among the most active tropical cyclone (TC) breeding grounds, with only four TCs per year^{1,2}, these BOB TCs can trigger serious tides, heavy rainfall and devastating wind in coastal regions^{3,4}. The BOB is surrounded by land on three sides with South Asian developing countries, for example, India, Myanmar, Bangladesh, and Sri Lanka, which are severely affected by TCs due to their dense population, shallow sea floor, and low-lying, flat terrains in the surrounding coastal regions^{5–7}. Occasionally, BOB TCs can even bring snowstorms to the Tibetan Plateau and cause heavy rainfall in Southwest and East China^{4,8}.

BOB TCs are usually active in the pre-monsoon (April–May) and post-monsoon seasons (October–December, also called late-season for the Northern Hemisphere TC season)^{7,9} but are relatively silent in-between due to the strong vertical wind shear brought by the South Asian summer monsoon^{2,7}. In particular, the post-monsoon seasons account for 64% of the annual TC frequency over the BOB (Fig. 1A). It has also been suggested that more intense TCs over the BOB generally form during the post-monsoon season⁷ when the vertical wind shear weakens and hydrographic conditions become favorable for TC genesis and development^{7,10,11}. Besides the above environmental conditions, it can be seen from Fig. 1B that the TCs over the South China Sea (SCS) have the ability to cross the southern Indochina Peninsula to enter the BOB, possibly also contributing to the TC activity in this region.

The SCS is also a TC breeding ground and is separated from the BOB by the Indochina Peninsula. The TC activity over the SCS also has distinct seasonal features; boreal autumn TCs tend to move westward and strike the Indochina Peninsula, while boreal summer TCs usually move northwestward to make landfall in East Asia^{12,13}. Therefore, TCs over the SCS may have a closer

connection with TCs over the BOB after summer. It was suggested that SCS TCs are even more active than those over the western North Pacific (WNP) during the late-season^{14–16}. Although TC activity in the SCS peaks in the summer months, late-season TCs can still account for 31% of the annual TC frequency in this region (Fig. 1A). Besides, similar to the BOB, the SCS is also surrounded by land. The geography of bay and sea leads to a short warning period for countries surrounding the bay and the sea¹⁶, requiring deeper understanding of TC variability there.

Previous studies have suggested that the tropical Indo-Pacific Oceans play important roles in modulating TCs in the BOB and the SCS^{9,17}. The El Niño–Southern Oscillation (ENSO), a dominant interannual variability in the Pacific Ocean, exerts important modulatory effects on TC genesis frequency, location, track, and landfall over the BOB. Compared to El Niño years, higher TC genesis frequency and longer TC lifetime over the BOB are observed during La Niña years because of the higher sea surface temperature (SST), reduced vertical wind shear, enhanced mid-level relative humidity, and low-level cyclonic circulation^{18–21}. In addition, the mean genesis location of TCs shifts eastward, with a tendency of more recurving tracks in La Niña years²². Similarly, above-normal TC frequency over the SCS appears during La Niña years compared to El Niño years, also due to warmer local SST, weakened vertical wind shear, more water vapour, and increased cyclonic low-level relative vorticity over the SCS^{15,23,24}.

In addition to the ENSO, the Indian Ocean Dipole (IOD), a zonal dipole mode of SST anomalies in the tropical Indian Ocean²⁵, can also cause significant BOB TC anomalies^{4,17,26}. During negative (positive) IOD events, enhanced (weakened) convection over the eastern Indian Ocean can induce cyclone (anticyclone) anomalies over the BOB, resulting in enhanced (weakened) low-level cyclonic vorticity and higher (lower) BOB TC genesis frequency⁴. Relative to studies on the impacts of the IOD on BOB TCs, little attention has

¹Ocean College, Zhejiang University, Zhoushan, China. ²Southern Marine Science and Engineering Guangdong Laboratory (Zhuhai), Zhuhai, China. ³State Key Laboratory of Satellite Ocean Environment Dynamics, Second Institute of Oceanography, Ministry of Natural Resources, Hangzhou, China. ⁴School of Atmospheric Sciences, Sun Yat-sen University, Zhuhai, China. ⁵Guangdong Province Key Laboratory for Climate Change and Natural Disaster Studies, Sun Yat-sen University, Zhuhai, China. ✉email: hucd@zju.edu.cn

been paid to the relationship between IOD and SCS TCs. More efforts have targeted the impacts of abnormal eastern and tropical Indian Ocean SST on WNP TCs, which can induce the Kelvin wave to its east and lead to anomalous cyclonic (anticyclonic) atmospheric circulation and increased (decreased) TC activity over the WNP^{27–31}.

Both Pacific and Indian Ocean SST anomalies can widely influence the atmospheric circulations over the BOB–SCS region. Therefore, it is reasonable to expect coherent changes in TC activity in this area when the Pacific and Indian Oceans are at play. Such potential interbasin TC covariability, however, has not been well explored⁹. In addition, the relative contributions of the Pacific and the Indian Ocean to TC anomalies are also unclear. In this study, we found a strong covariability of consistent changes in TC activity over the BOB and the SCS during the late-season (October–December). The inter-basin anomalies of TC can be modulated by an intrinsic tripole pattern of SST anomalies in the tropical Indo-Pacific. This finding can improve our understanding of regional TC activity and is beneficial to decision-makers, government policy and planning, as well as reducing losses for coastal residents, especially in developing coastal countries³².

RESULTS

Strong covariability of TCs between BOB and SCS

A total of 141 TCs occurred over the SCS during October–December between 1979–2019 (green TCs in Fig. 1B). These TCs can be divided into local TCs and migrated TCs (see methods for detailed definition for different types of TCs)³³. About 80% of SCS TCs (112 in 141) are migrated TCs, which indicate that they formed over the WNP, then moved westward and migrated to the SCS. Meanwhile, locally generated TCs over the SCS accounted for only a small proportion (29 in 141). A total of 113 TCs affected the BOB region, with 94 locally generated TCs over the BOB (blue TCs in Fig. 1B) and only 19 TCs migrating from the SCS to the BOB region (Fig. 1B). This shows the comparable frequency of TC activity between the two basins during the late-season. The time series of the frequency of these TCs are shown in Supplementary Fig. 1. As seen in Fig. 1C, TC activity shows large variations over the BOB and SCS. There are two track density centers, with one over the SCS and the other over the BOB. Figure 1B, C suggest that TCs over the WNP could take a westward track to the SCS region, while BOB TC activity may show a connection with SCS TC activity through the southern Indochina Peninsula.

Next, we applied maximum covariance analysis (MCA) to the regional TC track density to more specifically reveal the possible covariability of TC activities over the two basins (Fig. 2). The leading MCA mode (MCA1) explains 74.8% of the covariance between TC activities in these two areas during late-season. Figure 2A, B reflect the consistent change of TC track activity anomalies in the BOB and the SCS, respectively. The pattern of MCA1 for track density over the BOB (MCA1–BOB) includes a signal of TC activity over both the SCS west of 115°E and the southeast of the Philippines (Fig. 2A). On the other hand, the MCA1 for track density over the SCS (MCA1–SCS) is associated with TC anomalies over the northern and eastern BOB (Fig. 2B). The time series of MCA1–BOB and MCA1–SCS are highly correlated ($R = 0.71$, $p < 0.01$; Fig. 2D), and their 19-year sliding correlations are generally stable and significant (Supplementary Fig. 2). Thus, this MCA1 results indicate the strong covariability of the TC activity between the BOB and the SCS. Besides the connection in patterns, we can also find a significant relationship between the total TC frequency over the two basins ($R = 0.50$, $p < 0.01$; Supplementary Table 1).

The main features of inter-basin TC activities were obtained by applying empirical orthogonal function (EOF) analysis on track density over the whole BOB–SCS region (Fig. 2C). The first leading mode (EOF1) of track density, which explains 35.0% of TC track

density variance, combines the spatial features of the MCA1 mode in both basins, with feeble associated signals over the Arabian Sea and most of the WNP. The principal component of EOF1 (PC1; Fig. 2D) was highly correlated with the time series of both MCA1–BOB ($R = 0.94$, $p < 0.01$) and MCA1–SCS ($R = 0.86$, $p < 0.01$), illustrating that this PC1 also well captures the temporal features of TC track activity in both basins. During active and inactive TC years, the changes in frequency can reach 50% of the climatology (Supplementary Table 2), highlighting the strong variability of TC activity. This EOF1 mode further demonstrates the strong covariability of TC track activity over the two basins.

Local and migrated TCs are likely to be both connected to the covariability of TCs over the two basins. Thus, we calculated the correlation coefficients between the PC1 and the time series of TC frequencies (Supplementary Table 1). As expected, the PC1 had significant correlations not only with SCS local TCs ($R = 0.48$, $p < 0.01$) and migrated TCs ($R = 0.65$, $p < 0.01$), but also with BOB local TCs ($R = 0.67$, $p < 0.01$) and migrated TCs ($R = 0.48$, $p < 0.01$). These data show that the frequency of both these types of TCs in the two ocean basins can play a role in the overall TC activities, especially frequency, over the BOB–SCS regions.

A question arises that whether the BOB migrated TCs dominate the covariability between BOB TC and SCS TC. To answer this question, we exclude the parts (west of 100°E) of TC track data migrated from the SCS to the BOB region, and only keep these BOB migrated TC track data east of 100°E. The other TC track data remain unchanged. Then we perform the same analysis as in Fig. 2, the reproduced results are shown in Supplementary Fig. 3. It is clear that the covariability of BOB–SCS TC track activity remains very significant ($R = 0.64$, $p < 0.01$, Supplementary Fig. 3), albeit with some decrease relative to that of Fig. 2 ($R = 0.71$, $p < 0.01$). Moreover, the spatial patterns of Supplementary Fig. 3 are also consistent to those shown in Fig. 2. Besides, the leading EOF1 (Supplementary Fig. 3C) can also capture the covariability of BOB–SCS TC track activity after removing the influences of BOB migrated TCs. Hence, the migrated TCs from the SCS to the BOB indeed only contribute partly to increasing the covariability of BOB–SCS TC-track activity, but do not play a dominant role.

Modulatory effects of the Indo-Pacific Tripole

Herein, we applied the MCA method again to describe the relationship between overall TC track density over the BOB–SCS region (80°–115°E, 5°–30°N) and SST in the Indo-Pacific (40°E–80°W, 30°S–30°N) (Fig. 3). The correlation coefficient between the MCA1 for TC (MCA1–TC) and PC1 was 0.97 ($p < 0.01$; Fig. 3A). In addition, the track density pattern of the MCA1 (Fig. 3B) was almost identical to that of EOF1 (Fig. 2C). The pattern of MCA1 for SST (MCA1–SST) shows zonally tripolar SST anomalies in the tropical Indo-Pacific Ocean (Fig. 3C), which was identified as the negative phase of Indo-Pacific Tripole (IPT)³⁴, an intrinsic mode of tropical climate variability (see Method). The Pacific part of positive IPT mode is the classical El Niño pattern while the Indian Ocean part is almost identical to positive IOD mode (Supplementary Figs. 4 and 5). Given the correlation coefficient between the MCA1–SST and IPT index was -0.99 , we identified the MCA1–SST time series as the inverse IPT index. Namely, a positive value of MCA1–SST corresponds to a negative IPT (i.e., $-IPT$). The time series of $-IPT$ index and MCA1–TC are highly correlated ($R = 0.63$, $p < 0.01$; Fig. 3A), and their 19-year sliding correlations are also generally stable and significant (Supplementary Fig. 2). Consequently, this coupled MCA1 mode possibly represents the modulatory effect of the tropical Indo-Pacific IPT on the TC activity over the BOB–SCS region.

In the negative IPT phase, warmer WNP and eastern Indian Ocean, together with cooler western Indian Ocean and central–eastern Pacific, can lead to an enhanced Walker circulation (Fig. 4A). In line with the Walker circulation change, anomalously

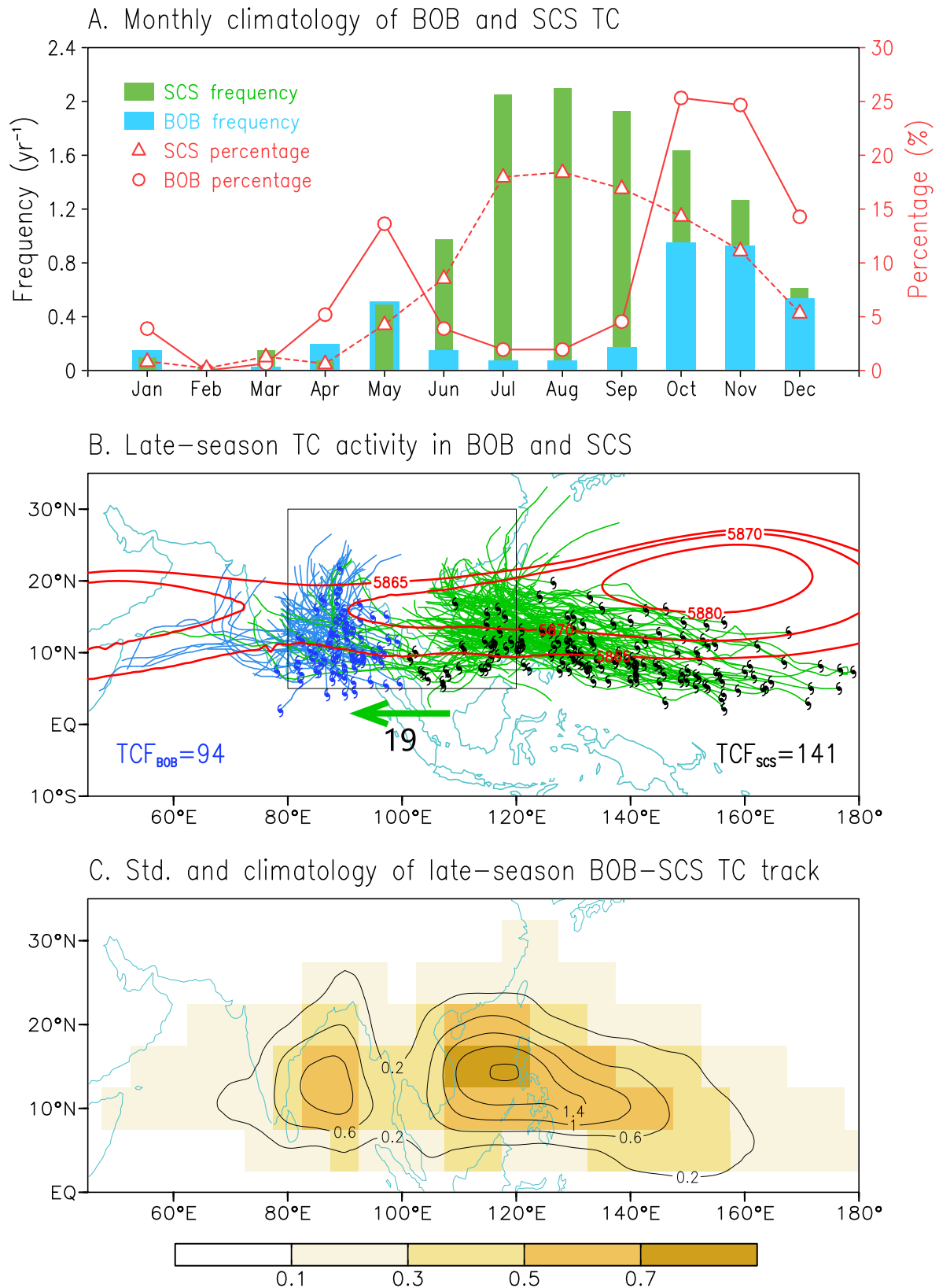


Fig. 1 Climatology of BOB-SCS TC during the late-season. **A** Monthly climatology of local TC frequency in the BOB (blue bar), TC frequency in the SCS (green bar), local TC percentage in the BOB (solid line with circle mark) and TC percentage in the SCS (dashed line with triangle mark) relative to the annual frequency. See methods for various TC definitions. **B** Genesis location and tracks of the local TC in the BOB (blue) and TC in the SCS (green) during late-season (October-December). The black rectangles outline the regions of BOB-SCS in this paper. **C** Standard deviation (shading) and climatology (contour; yr⁻¹) of late-season BOB-SCS TC track density.

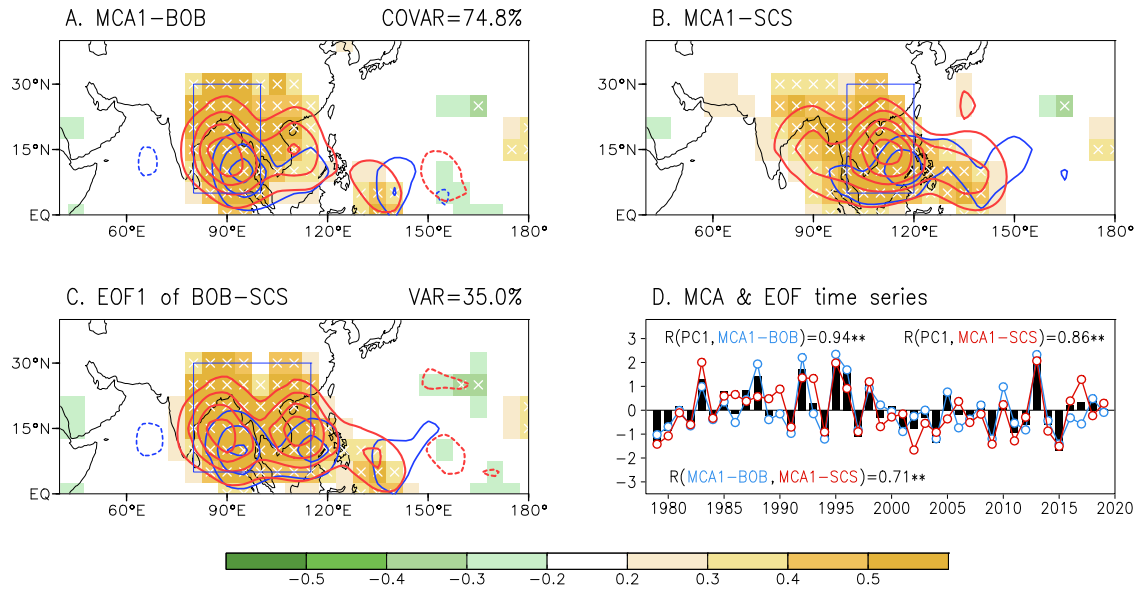


Fig. 2 Covariability of the BOB-SCS TC track density. Correlations of track density (shading), regression of track density (red contour, interval of 0.1 yr^{-1}), and regression of genesis density (blue contour, interval of 0.03 yr^{-1}) on the time series of first MCA mode of standardized track density over (A) the BOB (MCA1-BOB; 80° – 100°E , 5° – 30°N) and (B) the SCS (MCA1-SCS; 100° – 120°E , 5° – 30°N). C The same as (A) but onto the principal component (PC1) of first leading mode (EOF1) of standardized track density over the BOB-SCS (80° – 115°E , 5° – 30°N). Cross indicates that correlations are significant at the 0.05 significance level. D Time series of MCA1-BOB (blue), MCA1-SCS (red) and PC1 (black). The correlation coefficients between them are given, with “**” indicating that the correlations exceed the 0.01 significance level.

ascending motions cover the regions of the BOB–western WNP, where the atmospheric conditions can be favorable for TC activity with enhanced convection. However, over the Arabian Sea and the Pacific east of 150°E , stronger descending motions can bring an unfavorable environment for TC activity. Change in the Hadley circulation features two ascending motion centers located on both sides of the equator and a forced downdraft over the subtropics of the Northern Hemisphere (20° – 30°N) (Fig. 4B).

These large-scale atmospheric circulation changes suggest that there is more active convection over the Maritime Continent responding to warmer SST. As seen in Fig. 4C, increased precipitation occurs over the BOB–western WNP. The anomalous tropical heating released by this precipitation leads to a Matsuno-Gill pattern: an anomalous cyclone in the lower–middle-level atmosphere over the BOB-SCS (Fig. 4D, E) and an anomalous anticyclone in the upper-level atmosphere (Fig. 4F) over the South Asia. Lower-level cyclonic circulation anomalies over the BOB-SCS region are favorable for TC activity by altering dynamical or thermodynamical conditions, which will be analyzed next. While over the eastern WNP, decreased precipitation, lower-level anticyclonic circulation and upper-level cyclonic circulation all suggest a suppressed TC activity. As can be seen in Fig. 4E, the easterly steering flow over the WNP is conducive to the westward movement of TCs into the SCS, while the westerly steering flow over the southern part of the Indochina Peninsula is unfavorable for the westward movement of TCs into the BOB.

For the negative IPT phase, due to the wind change between upper and lower levels (Fig. 4D, F), the vertical wind shear significantly increases (decreases) over the southern (northern) part of the BOB-SCS region (Fig. 5A). On the other hand, the cyclone with low/mid-level anomalies suggests that the environment generally becomes favorable for TC activity over the BOB–western WNP region. For example, the 850-hPa relative vorticity, 500-hPa meridional gradient of zonal wind, and vertical velocity all show consistent changes conducive for TC genesis (Fig. 5B–D). The opposite effects are seen over the eastern WNP. The overall effects of the above variables can be demonstrated by the dynamic genesis potential index (DGPI): negative IPT induces

increased DGPI from the BOB to the western WNP but decreased DGPI over the eastern WNP (Fig. 5E). Therefore, the evaluation of DGPI suggests that environmental conditions are favorable (unfavorable) for TC genesis over the BOB–western WNP (eastern WNP) in the presence of negative IPT. The DGPI patterns are generally consistent with the genesis density anomalies over the BOB-SCS region (Fig. 5E). Although DGPI excludes mid-level relative humidity, previous studies suggest that TC genesis over the BOB and SCS is also modulated by mid-level moisture^{35,36}. Thus, the increased humidity indicates favorable conditions over the BOB–western WNP (Fig. 5F), similar to the patterns of vertical velocity (Fig. 5D).

Discrepancy in the locally-generated and migrated TCs

In the former section, we indicated that both local and migrated TCs can contribute to the EOF1 of BOB-SCS TC track activity. However, whether these two types of TCs change significantly with the IPT is still unclear. We selected the strongest positive and negative 11-year inverse IPT index anomalies to answer this question and further investigate why the IPT failed to significantly alter the frequency of BOB and SCS migrated TCs (Table 1). The local TCs over both basins were higher (lower) than the climatology associated with the negative (positive) IPT. The differences in these local TCs between positive and negative years were significant ($p < 0.05$; Table 1). However, the frequency of BOB or SCS migrated TCs did not significantly change with the IPT phases ($p > 0.1$). This suggests that the IPT may only significantly change the local TC genesis frequency to contribute to the covariability of BOB-SCS TC track activity.

The significant changes in steering flow over the western WNP to the southern Indochina Peninsula (Fig. 4E) suggest that the IPT should have modulated the migrated TC movement as described previously. But the IPT is not significantly linked to the frequency of the migrated TCs (Table 1, Supplementary Table 1 and Supplementary Figs. 6, 7), which is not consistent with the significant steering flow changes, prompting further investigation. Thus, the composite of migrated TC and the subtropical high

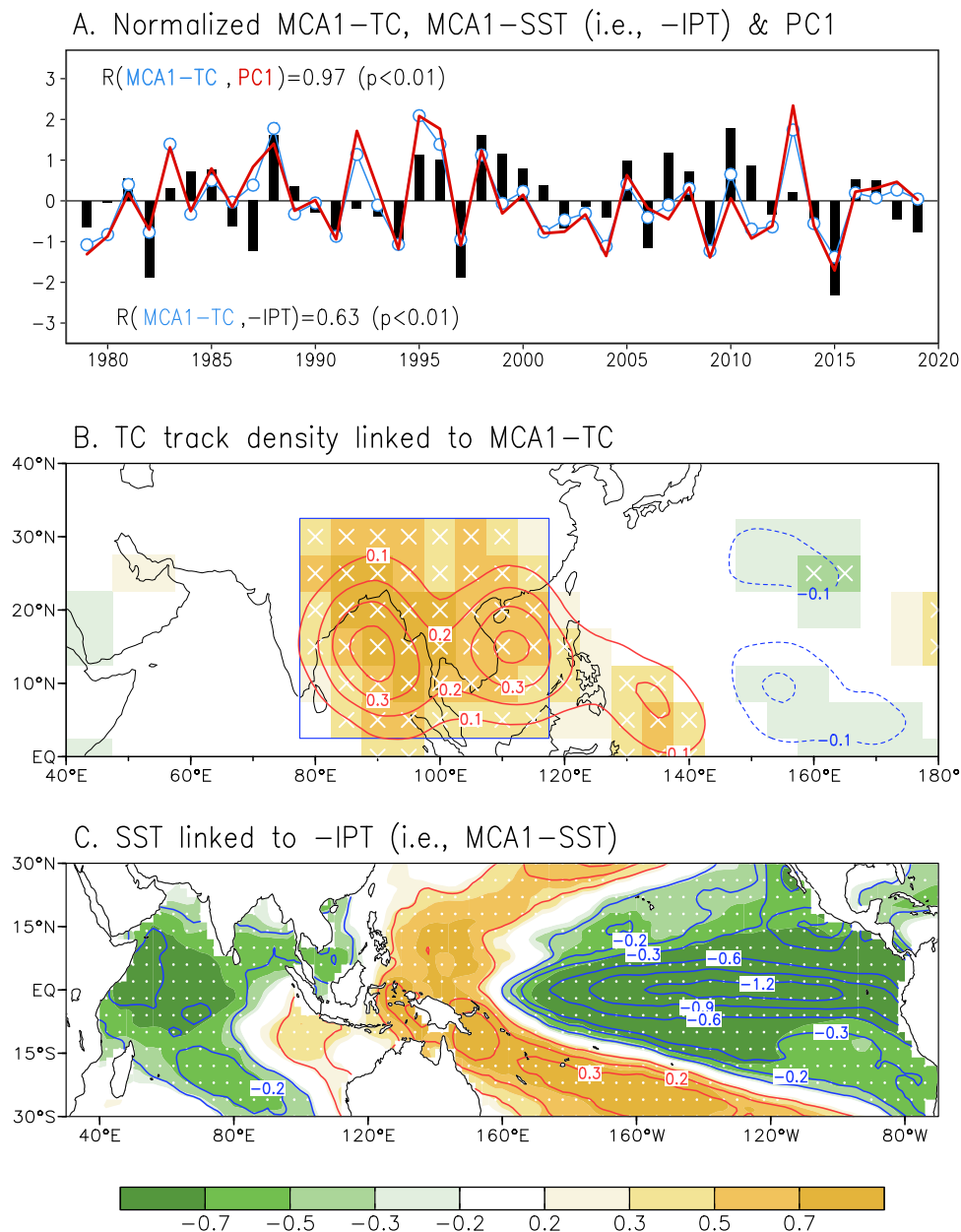


Fig. 3 Linkage between the BOB–SCS TC track activity and the tropical Indo-Pacific SST. **A** Time series of first MCA mode for BOB–SCS TC track density (blue; MCA1–TC) and tropical Indo-Pacific SST [black; MCA1–SST (i.e., –IPT)], and the time series of PC1 (red). The correlation coefficients between them and corresponding significance level (i.e., p -value) of two tailed Student’s t -test are given. **B** and **C** show the correlation (shading) and regression (contour, interval of 0.1, zero contour omitted) patterns of TC track density on MCA1–TC and those of SST ($^{\circ}$ C) on the –IPT time series, respectively. Stippling and cross indicate that correlations pass the 0.05 significance level.

under different IPT phases were shown in Fig. 6. In negative IPT years, more migrated TC were generated in the SCS and the western WNP (Fig. 6A). Although the subtropical high weakened and retreated eastward, it was still able to drive these TCs westward into the SCS or the BOB. In positive IPT years, although the genesis locations of these migrated TCs were more easterly, the subtropical high also became stronger (Fig. 6B). A strong subtropical high is conducive to stably guiding these migrated TC westward, eventually making them enter the SCS or the BOB. The difference in the longitude of migrated TC genesis reached 10.74° ($p < 0.01$) between different IPT phases. In other words, although IPT affected the mean genesis location of TCs over the SCS–WNP, shown as the zonal contrast (west positive and east negative) of TC genesis (Fig. 5E), these TCs were heading westward under the

guidance of atmospheric circulation and did not trigger a significant change in the migrated TC frequency.

The change in the frequency of SCS migrated TCs is actually related to the genesis of TCs over both the western and eastern WNP (Supplementary Fig. 6C). In the atmospheric circulation field, the increase in SCS migrated TCs can be linked to the high pressure anomalies in the subtropics from the WNP to Asia (Supplementary Fig. 6D). This abnormal belt of high pressure can act as a wall favorable for more WNP TCs to move westward. For BOB migrated TCs, they were found to be not significantly associated with changes in the atmospheric circulation (Supplementary Fig. 7A, B and D). Interestingly, the genesis of TCs associated with the BOB migrated TCs exhibited a zonal alternation pattern (Supplementary Fig. 7C). This feature may

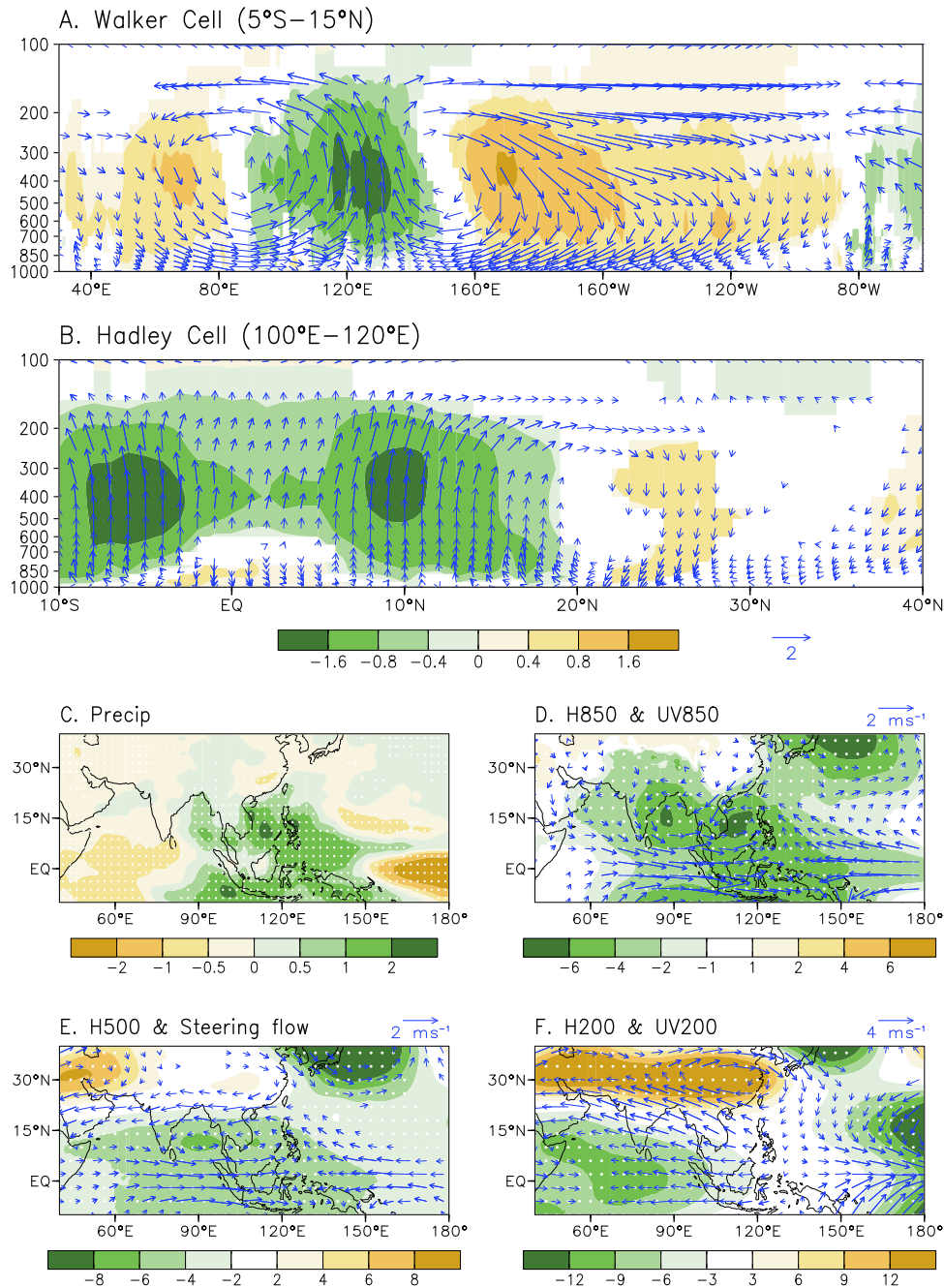


Fig. 4 IPT-related tropical circulation and precipitation anomalies. Regressions on the inverse IPT for **(A)** Walker cell averaged between 5°S and 15°N, **(B)** Hadley cell averaged between 100°E and 120°E (shaded for the corresponding regressed vertical velocity, units: $10^{-2} \text{ Pa s}^{-1}$), **(C)** precipitation (mm day^{-1}), **(D)** geopotential height (shading; gpm), and horizontal wind (vector; m s^{-1}) at 850 hPa, **(E)** geopotential height (shading; gpm) at 500 hPa and steering flow (vector; m s^{-1}), **(F)** geopotential height (shading; gpm) and horizontal wind (vector; m s^{-1}) at 200 hPa. The vector and stippling indicate that regressions are significant at the 0.05 significance level.

reflect the TC activity at a smaller spatiotemporal scale and thus may be affected by the intraseasonal process.

DISCUSSIONS

Our results reveal that the BOB–SCS TC track activity during the late-season shows strong inter-basin covariability. The leading mode explains approximately 35% of the variance in TC track activity over the BOB–SCS, the corresponding changes in BOB–SCS TC frequency can exceed 50% of the climatology. Further, this TC

covariability is significantly modulated by the IPT mode. When the IPT-related SST anomalies exhibit a zonally negative-positive-negative pattern, i.e., a combination of negative IOD and La Niña, TC activity over the BOB–SCS region is promoted by the anomalous cyclonic circulation in the overlying atmosphere. As a result, atmospheric variables, such as lower-level relative vorticity, mid-level meridional gradient of zonal wind and mid-level vertical velocity, become favorable for local TC genesis. On the other hand, for migrated TCs, the IPT mainly regulates their genesis location but not their frequency. Moreover, the migrated

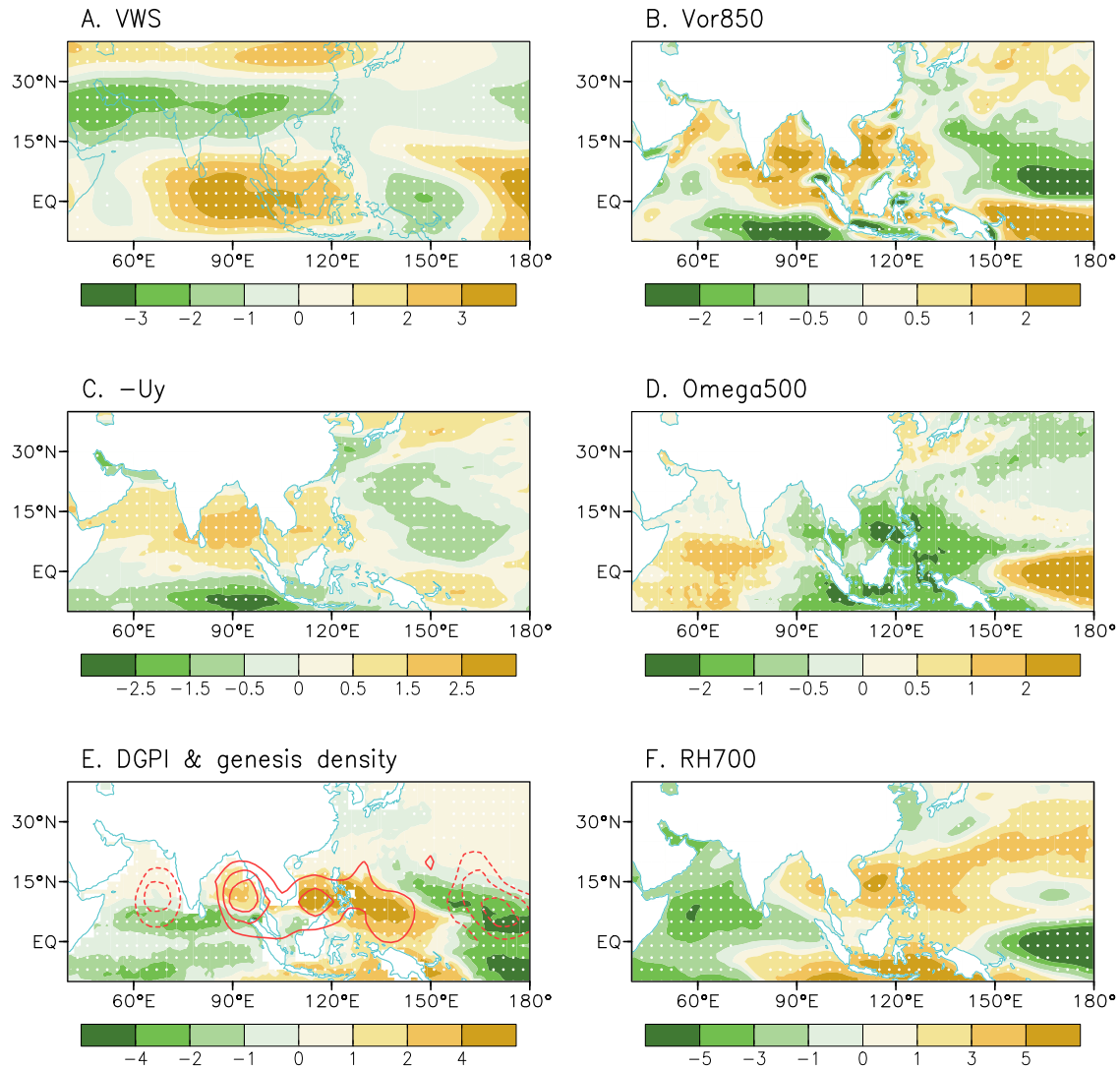


Fig. 5 IPT-related environmental conditions for TC genesis. Regressions on the inverse IPT for (A) vertical wind shear (m s^{-1}), (B) 850-hPa relative vorticity (10^{-6} s^{-1}), (C) 500-hPa meridional gradient of zonal wind (10^{-6} s^{-1}), (D) 500-hPa vertical velocity ($10^{-2} \text{ Pa s}^{-1}$), (E) dynamic genesis potential index (shading) and genesis density (contour, interval of 0.02 yr^{-1}), and (F) 700-hPa relative humidity (%). Stippling indicates that regression is significant at the 0.05 significance level.

Table 1. Composite frequency of TCs in different phases of IPT.

Groups \ Frequency (yr^{-1})	LTC _{BOB}	MTC _{BOB}	LTC _{SCS}	MTC _{SCS}
Climatology, OND 1979–2019	2.29	0.46	0.71	2.73
Negative IPT 1985, 1988, 1995, 1996, 1998, 1999, 2000, 2005, 2007, 2010, 2011	3.00	0.45	1.00	2.55
Positive IPT 1979, 1982, 1987, 1991, 1994, 1997, 2002, 2006, 2009, 2015, 2019	1.73	0.27	0.18	2.36
Difference	1.27*	0.18	0.82*	0.19

The selected years were the 11 years with the strongest negative or positive IPT index anomalies. LTC (MTC) denotes the local (migrated) TC and the subscript indicates the basin; Bold values with “*” mean that the difference of averaged TC frequency between positive and negative index years passes the 0.05 significance level.

TCs from the SCS to the BOB only contribute partly to increasing the covariability of the BOB–SCS TC-track activity, but not play a dominant role.

One might wonder about the relationship between IPT and ENSO, and their differences in modulating BOB–SCS TCs. Although the $-IPT$ (i.e., the MCA1–SST) reflects the ENSO pattern to a large

extent (Fig. 3C vs Supplementary Fig. 8A), only the ENSO signal in the Pacific cannot entirely explain the influence of tropical Indo-Pacific SST anomalies on climate variations³⁷. Previous studies have compared the features of IPT and ENSO, as well as their influences on the climate in China and the rainfall in India using observations and numerical experiments. It was confirmed that

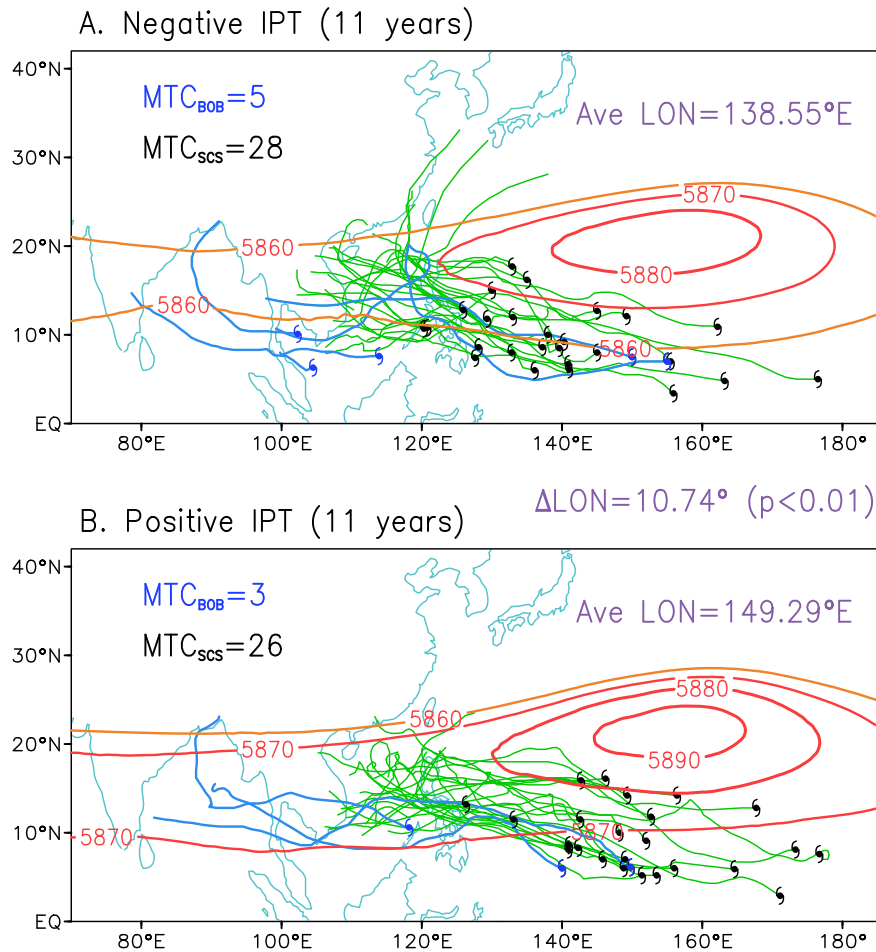


Fig. 6 Migrated TC in anomalous IPT years. SCS (black dot and green curve) and BOB (blue dot and curve) migrated TC (MTC, the subscript indicates the basin) during (A) negative IPT years and (B) positive IPT years. The average genesis longitude (LON) of all drawn TCs is marked in the upper right corner. The red contours represent the WNP subtropical high (represented by geopotential height) at 500 hPa.

the influences of IPT are different from that of ENSO and IOD^{37,38}, because the ENSO and IOD cannot contain all of each other's signals (see Supplementary Fig. 8C, D). Compared to the ENSO pattern (Supplementary Fig. 8A), the $-IPT$ (i.e., the MCA1-SST) mode can indeed better represent SST anomaly signals especially in the tropical western Indian Ocean (Fig. 3C)^{34,39}. Accordingly, the advantage of IPT over the Niño3.4 index in connecting BOB–SCS TC covariance is well-founded. The IPT generally possesses better correlations with BOB–SCS TC compared to the Niño3.4 index (Supplementary Table 3). Also as shown in Supplementary Table 4, when the Niño3.4 is used to replace the IPT, the composite difference in BOB local TC frequency becomes insignificant, dropped from 1.27 ($p < 0.05$, Table 1) to 0.45 ($p > 0.1$, Supplementary Table 4).

It is no doubt that the pantropical interactions make it challenging to clarify the relative importance of the contributions of the Pacific and Indian oceans. Nonetheless, the relative role of SST in the Pacific and Indian oceans can be calculated if the SST is prescribed in the atmospheric-only numerical simulation while ignoring the interactions between the ENSO and the IOD. Herein, sensitive experiments were designed with anomalous SST forcing using the Community Atmosphere Model version 4 (CAM4) to confirm the modulatory effects and relative contributions of the SST of tropical Indian and Pacific oceans on the BOB–SCS atmospheric circulations (see Supplementary Fig. 9 and Numerical experiment in Methods). The simulations generally reproduced the observed modulatory effects of the IPT on the BOB–SCS atmospheric circulations. These

modulatory effects of SST anomalies on the atmospheric circulations are diagnosed by the lower-level relative vorticity in CAM4 (Fig. 7), because the vorticity well represents the distributions of TC genesis anomalies (Fig. 5E) and is a good indicator of cyclonic circulation. Here, the intensity of anomalous cyclone is defined as the averaged relative vorticity in the red box. We can find that the Indo-Pacific SST experiment generated the strongest cyclone (relative vorticity = $1.06 \times 10^{-6} \text{ s}^{-1}$; Fig. 7A). This is because the SST gradient between the Indian and the Pacific oceans is the strongest. Both the Indian Ocean and Pacific SSTs can contribute to the anomalous cyclonic circulations over the BOB–SCS region. Compared with the Indian Ocean (Fig. 7B), however, SST anomalies in the Pacific can promote stronger low-level cyclones to modulate TC activity (Fig. 7C). In the Pacific SST experiment, the intensity of cyclonic vorticity was $0.91 \times 10^{-6} \text{ s}^{-1}$, which is about twice that of the Indian Ocean SST experiment (relative vorticity = $0.45 \times 10^{-6} \text{ s}^{-1}$). The sum of these two vorticities is notably larger than that in the Indo-Pacific experiment, possibly due to the non-linearly mutual process of modulatory effects of Indo-Pacific Oceans. These results suggest that the Pacific SST anomalies are much more important than the Indian Ocean SST anomalies.

Although the spectral analysis (Supplementary Fig. 10) demonstrated that the leading mode of BOB–SCS TC track activity exhibits mainly interannual variability in 2.5-yr periods during 1979–2019, the PC1 shifted from positive to negative in the late-1990s (Fig. 2D), possibly suggesting an interdecadal variation of BOB–SCS TCs. At the interdecadal scale, the Indo-Pacific SST plays an important role in

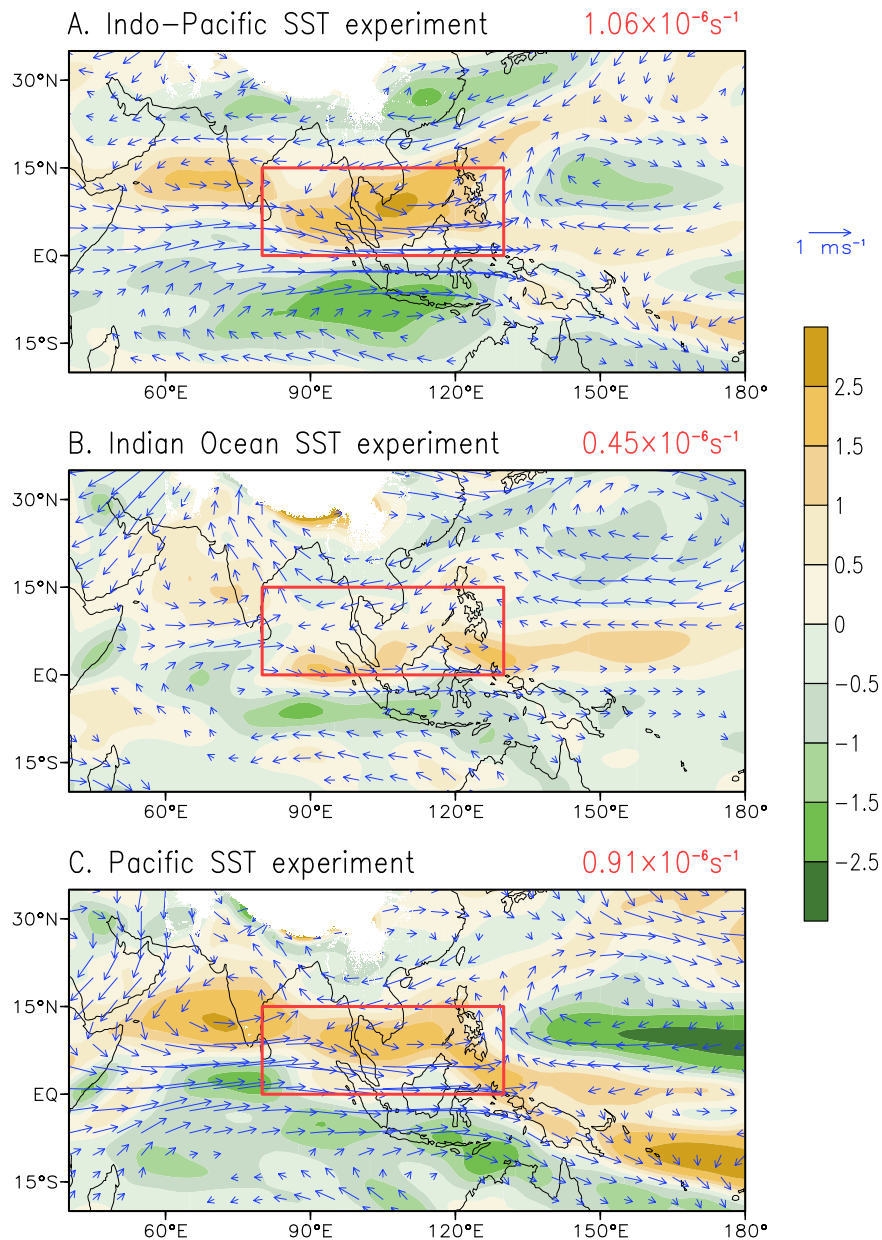


Fig. 7 Numerical experiment results. CAM4 simulations for 850-hPa relative vorticity (shading; 10^{-6} s^{-1}) and steering flow (vector; m s^{-1}) forced by (A) Indo-Pacific SST anomalies, (B) Indian Ocean SST anomalies, and (C) Pacific SST anomalies. The results are shown as the difference between each sensitive run and the CTRL. The averaged relative vorticity in the red rectangle (80° – 130°E , 0° – 15°N) is given at the upper right corner.

the BOB–SCS TC similar to the interannual timescale. For example, previous studies have documented that the Pacific decadal oscillation can modulate BOB TCs^{40,41} and SCS TCs^{24,42,43}. SCS TCs are also affected by the SST variability of the Indian Ocean at the interdecadal timescale³⁰. Besides, intraseasonal oscillations, for instance, the Madden-Julian oscillation and the quasi-biweekly oscillation, over the Indo-Pacific warm pool can also have major roles. As these intraseasonal oscillations either promote or inhibit convection over the tropical oceans, they significantly modulate TC activities over the BOB^{44,45} and the SCS^{13,46–48}. For example, a recent study suggested that the active TC genesis tends to be observed over the WNP in the late withdrawal years of the SCS summer monsoon⁴⁹, which may also indirectly modulate the BOB–SCS TC covariability. Thus, it is needed to further investigate how the diverse modulators at different timescales mutually influence the TC activity over the BOB–SCS in the future.

METHODS

Observation-based data

Data for the BOB and SCS TCs during 1979–2019 were extracted from the Joint Typhoon Warning Center (JTWC) best-track data, a part of the International Best Track Archive for Climate Stewardship (IBTrACS), which includes information of TC latitude and longitude, 1-min average maximum sustained wind speed and center minimum sea-level pressure. To confirm the robustness of Fig. 2, we further reproduced the Supplementary Fig. 11 by using the TC best-track data (east to 100°E) obtained from the Shanghai Typhoon Institute of China Meteorological Administration (CMA) to replace the corresponding JTWC TC data (see the caption of Supplementary Fig. 11 for details). For atmospheric fields, we used the data from the European Centre for Medium-Range Weather Forecasts (ECMWF) reanalysis 5 (ERA5)⁵⁰. For SST data, the NOAA

Extended Reconstructed SST version 5 (ERSSTv5, $2^\circ \times 2^\circ$)⁵¹ and the Hadley Centre Global SST version 1.0⁵² (interpolated to the same $2^\circ \times 2^\circ$) were merged to ensure the reliability of SST data⁵³. Two SST indicators monitoring the IOD and ENSO, namely, the Dipole Mode Index and Niño3.4 index, were obtained from https://psl.noaa.gov/gcos_wgsp/Timeseries/DMI/ and <https://psl.noaa.gov/data/correlation/nina34.data>, respectively.

TC data processing

In the current study, only the TCs with peak wind speed greater than the tropical storm intensity threshold ($V_{\max} > 33$ knots) were considered. TC genesis was marked by the first record in the best-track data. TC genesis and track density were represented as the occurrence frequency of TC location data in $5^\circ \times 5^\circ$ box. Spatial smoothing was applied to the density data because the influence of TCs exists in a wide range. Each grid point was taken a weighted average of the grid point itself, plus eight surrounding points, with the center point receiving a weight of 1.0, the points on each side and above and below receiving a weight of 0.5, and corner points receiving a weight of 0.3.

Definitions of various TCs

The BOB TCs are selected over the region (80° – 100° E, 5° – 30° N), while the SCS TCs are selected over the region (100° – 120° E, 5° – 30° N) unless otherwise stated. For TC activities in a specific basin, they could refer to locally generated TCs (local TC; LTC) or TCs coming from another region (migrated TC; MTC). For convenience, these two types of TCs are defined as follows: if a TC is generated west (east) of 100° E and entered the BOB region, it was defined as a BOB local (migrated) TC; if a TC was generated within the SCS region (was generated east of 120° E and entered the SCS region), it was defined as a SCS local (migrated) TC. Some SCS migrated TCs can be BOB migrated TCs at the same time because they further move into the BOB region. Therefore, the BOB–SCS total TCs include the BOB local TCs, the SCS local TCs and the SCS migrated TCs, but exclude the BOB migrated TCs.

Statistical method and significance test

The long-term trends in the data were removed by linear regression methods. Two-tailed Student's *t*-test was used to evaluate the significance level of composite analysis, Pearson correlation and linear regression. Maximum covariance analysis (MCA), also known as singular value decomposition (SVD), was implemented to identify the pair of patterns that explain the maximum fraction of covariance among variables⁵⁴. Empirical orthogonal function (EOF), also known as principal component analysis (PCA), was utilized to identify the patterns explaining the highest fraction of variability⁵⁵.

The influence of atmospheric circulation on the TC track is represented by the steering flow, which is defined as the pressure-weighted wind averaged from 850 to 300 hPa⁵⁶. To diagnose the influence of atmospheric environmental conditions on TC genesis, we employ the dynamic genesis potential index (DGPI)⁵⁷. The DGPI is calculated as follows:

$$DGPI = (2 + 0.1 \times VWS)^{-1.7} \left(5.5 - \frac{\partial u_{500}}{\partial y} \times 10^5 \right)^{2.3} (5 - 20 \times \omega_{500})^{3.3} (5.5 + |\eta_{850} \times 10^5|)^{2.4} e^{-11.8} - 1 \quad (1)$$

where *VWS* represents the vertical wind shear between 200 and 850 hPa, $\frac{\partial u_{500}}{\partial y}$ represents the meridional gradient of 500-hPa zonal wind, ω_{500} denotes the 500-hPa vertical velocity, and η_{850} denotes 850-hPa absolute vorticity. The DGPI was reported to have superiority over the most widely-used GPI^{58,59} in the WNP and the North Indian Ocean⁵⁷, which was also confirmed by our

results. Therefore, we only present the results of DGPI in this paper.

Definition of Indo-Pacific Tripole

Chen³⁴ documented that there is an intrinsic mode of tripolar SST anomaly over the tropical Indo-Pacific Oceans during the boreal autumn, namely, the Indo-Pacific Tripole. Chen depicted this tripole as the first-mode (MVEOF1) multivariate empirical orthogonal function (MVEOF) of sea surface temperature, sea surface height and surface wind stress for the tropical Indo-Pacific region (30° E– 70° W, 20° S– 20° N) during the September–November (SON) season. For convenience, we calculated the MVEOF1 using sea surface temperature and horizontal surface wind in the same domain. The IPT patterns (Supplementary Fig. 4) are almost identical to those in the Fig. 1 of Chen³⁴. More details of the comparison between Chen's definition and our results are presented in Supplementary Note 1. A positive IPT pattern combines the SST anomalies of El Niño and positive IOD (Supplementary Figs. 4 and 5), exactly in the opposite phase of MCA1–SST (Fig. 3C). Therefore, we use the MCA1–SST as the inverse IPT index in this study, unless otherwise stated.

Numerical experiments

The numerical model from the National Center for Atmospheric Research (NCAR) Community Earth System Model version 1.2.2 (CESM1.2.2) with a resolution of $1.9^\circ \times 2.5^\circ$ was used to investigate the tropical Indo-Pacific SST impacts on the atmospheric circulations. The Community Atmosphere Model version 4 (CAM4) is the atmospheric component of CESM1.2.2. The control run (CTRL) was conducted with climatological monthly SST, sea ice and gas concentrations, which were all 1982–2001 averages⁶⁰. CTRL and sensitive experiments were integrated for 30 years, and the seasonal mean outputs of the last 25 years were used for analysis. The sensitive experiments were identical to the CTRL, except that the climatic SST was superimposed with anomalous SST obtained by regression. The forcing of anomalous SST is represented by the difference between the sensitive run and the CTRL (sensitive run minus CTRL). In the first sensitive experiment, the oceanic forcing was 1.5 times the tropical Indo-Pacific SST anomaly regression against the inverse IPT index during the late-season (Supplementary Fig. 9A). Outside the tropical Indo-Pacific, the atmosphere is forced by the climatic SST. Then, we further divided this SST anomaly into the Indian Ocean part and the Pacific part by 120° E to force the atmospheric circulation in the Indian Ocean SST experiment (Supplementary Fig. 9B) and the Pacific SST experiment (Supplementary Fig. 9C), respectively.

DATA AVAILABILITY

Data used in this study are all available online: the JTWC TC best-track data (<https://www.metoc.navy.mil/jtwc/jtwc.html?best-tracks>), the CMA TC best-track data (<https://tcdata.typhoon.org.cn/en/zjljsjj.html>), the ERA5 dataset (<https://www.ecmwf.int/en/forecasts/dataset/ecmwf-reanalysis-v5>), monthly precipitation data from the Global Precipitation Climatology Project (<https://psl.noaa.gov/data/gridded/data.gpcp.html>), NOAA ERSSTv5 data (<https://www.esrl.noaa.gov/psd/data/gridded/data.noaa.ersst.v5.html>), and the Hadley Centre Sea Ice and Sea Surface Temperature data (<https://www.metoffice.gov.uk/hadobs/hadisst/>).

CODE AVAILABILITY

The source codes used to produce these results are available from the corresponding author upon reasonable request. The CESM model can be downloaded from <http://github.com/ESCOMP/CESM>.

Received: 10 July 2023; Accepted: 18 October 2023;
Published online: 07 November 2023

REFERENCES

- Alam, M. M., Hossain, M. A. & Shafee, S. Frequency of Bay of Bengal cyclonic storms and depressions crossing different coastal zones. *Int. J. Climatol.* **23**, 1119–1125 (2003).
- Hoarau, K., Bernard, J. & Chalonge, L. Intense tropical cyclone activities in the Northern Indian Ocean. *Int. J. Climatol.* **32**, 1935–1945 (2012).
- Lin, I. I., Chen, C. H., Pun, I. F., Liu, W. T. & Wu, C. C. Warm ocean anomaly, air sea fluxes, and the rapid intensification of tropical cyclone Nargis (2008). *Geophys. Res. Lett.* **36**, L3817 (2009).
- Yuan, J. & Cao, J. North Indian Ocean tropical cyclone activities influenced by the Indian Ocean Dipole mode. *Sci. China Earth Sci.* **56**, 855–865 (2013).
- Webster, P. J. Myanmar's deadly daffodil. *Nat. Geosci.* **1**, 488–490 (2008).
- Islam, T. & Peterson, R. E. Climatology of landfalling tropical cyclones in Bangladesh 1877–2003. *Nat. Hazards* **48**, 115–135 (2009).
- Balaguru, K., Taraphdar, S., Leung, L. R. & Foltz, G. R. Increase in the intensity of postmonsoon Bay of Bengal tropical cyclones. *Geophys. Res. Lett.* **41**, 3594–3601 (2014).
- Arakane, S. et al. Remote effect of a tropical cyclone in the Bay of Bengal on a heavy-rainfall event in subtropical East Asia. *npj Clim. Atmos. Sci.* **2**, 25 (2019).
- Yuan, J., Gao, Y., Feng, D. & Yang, Y. The zonal dipole pattern of tropical cyclone genesis in the Indian Ocean influenced by the tropical Indo-Pacific ocean sea surface temperature anomalies. *J. Clim.* **32**, 6533–6549 (2019).
- Sengupta, D., Goddalahundi, B. R. & Anitha, D. S. Cyclone-induced mixing does not cool SST in the post-monsoon north Bay of Bengal. *Atmos. Sci. Lett.* **9**, 1–6 (2008).
- McPhaden, M. J. et al. Ocean-atmosphere interactions during cyclone Nargis. *Eos Trans. Am. Geophys. Union* **90**, 53–54 (2009).
- Wu, Z. et al. Distinct interdecadal change contrasts between summer and autumn in latitude-longitude covariability of Northwest Pacific typhoon genesis locations. *Geophys. Res. Lett.* **48**, e2021GL093494 (2021).
- Luo, X. et al. The decadal variation of eastward-moving tropical cyclones in the South China Sea during 1980–2020. *Geophys. Res. Lett.* **49**, e2021GL096640 (2022).
- Lin, Y. & Lee, C. An analysis of tropical cyclone formations in the South China Sea during the late season. *Mon. Weather Rev.* **139**, 2748–2760 (2011).
- Shi, Y., Du, Y., Chen, Z. & Zhou, W. Occurrence and impacts of tropical cyclones over the southern South China Sea. *Int. J. Climatol.* **40**, 4218–4227 (2020).
- Lin, Y., Teng, H., Hsieh, Y. & Lee, C. Tropical cyclone formation within strong northeasterly environments in the South China Sea. *Atmosphere* **12**, 1147 (2021).
- Mahala, B. K., Nayak, B. K. & Mohanty, P. K. Impacts of ENSO and IOD on tropical cyclone activity in the Bay of Bengal. *Nat. Hazards* **75**, 1105–1125 (2015).
- Girishkumar, M. S. & Ravichandran, M. The influences of ENSO on tropical cyclone activity in the Bay of Bengal during October–December. *J. Geophys. Res. Oceans* **117**, C2033 (2012).
- Felton, C. S., Subrahmanyam, B. & Murty, V. S. N. ENSO-modulated cyclogenesis over the Bay of Bengal. *J. Clim.* **26**, 9806–9818 (2013).
- Ng, E. K. & Chan, J. C. Interannual variations of tropical cyclone activity over the North Indian Ocean. *Int. J. Climatol.* **32**, 819–830 (2012).
- Roose, S., Ajayamohan, R. S., Ray, P., Mohan, P. R. & Mohanakumar, K. ENSO influence on Bay of Bengal cyclogenesis confined to low latitudes. *npj Clim. Atmos. Sci.* **5**, 31 (2022).
- Bhardwaj, P., Pattanaik, D. R. & Singh, O. Tropical cyclone activity over Bay of Bengal in relation to El Niño–Southern Oscillation. *Int. J. Climatol.* **39**, 5452–5469 (2019).
- Zuki, Z. M. & Lupo, A. R. Interannual variability of tropical cyclone activity in the southern South China Sea. *J. Geophys. Res. Atmos.* **113**, D6106 (2008).
- Goh, A. Z. & Chan, J. C. Interannual and interdecadal variations of tropical cyclone activity in the South China Sea. *Int. J. Climatol.* **30**, 827–843 (2010).
- Saji, N. H., Goswami, B. N., Vinayachandran, P. N. & Yamagata, T. A dipole mode in the tropical Indian Ocean. *Nature* **401**, 360–363 (1999).
- Singh, V. K. & Roxy, M. K. A review of ocean-atmosphere interactions during tropical cyclones in the North Indian Ocean. *Earth-Sci. Rev.* **226**, 103967 (2022).
- Du, Y., Yang, L. & Xie, S. Tropical Indian Ocean influence on Northwest Pacific tropical cyclones in summer following strong El Niño. *J. Clim.* **24**, 315–322 (2011).
- Zhan, R., Wang, Y. & Lei, X. Contributions of ENSO and east Indian Ocean SSTA to the interannual variability of Northwest Pacific tropical cyclone frequency. *J. Clim.* **24**, 509–521 (2011).
- Zhan, R., Wang, Y. & Wu, C. Impact of SSTA in the east Indian Ocean on the frequency of Northwest Pacific tropical cyclones: a regional atmospheric model study. *J. Clim.* **24**, 6227–6242 (2011).
- Wang, L., Huang, R. & Wu, R. Interdecadal variability in tropical cyclone frequency over the South China Sea and its association with the Indian Ocean sea surface temperature. *Geophys. Res. Lett.* **40**, 768–771 (2013).
- Gao, J. et al. Possible influence of tropical Indian Ocean sea surface temperature on the proportion of rapidly intensifying western North Pacific tropical cyclones during the extended boreal summer. *J. Clim.* **33**, 9129–9143 (2020).
- Wahiduzzaman, M., Oliver, E. C., Wotherspoon, S. J. & Holbrook, N. J. A climatological model of North Indian Ocean tropical cyclone genesis, tracks and landfall. *Clim. Dyn.* **49**, 2585–2603 (2017).
- Ling, Z., Wang, G. & Wang, C. Out-of-phase relationship between tropical cyclones generated locally in the South China Sea and non-locally from the Northwest Pacific ocean. *Clim. Dyn.* **45**, 1129–1136 (2015).
- Chen, D. Indo-Pacific tripole: an intrinsic mode of tropical climate variability. *Adv. Geosci.* **24**, 1–18 (2011).
- Li, Z., Li, T., Yu, W., Li, K. & Liu, Y. What controls the interannual variation of tropical cyclone genesis frequency over Bay of Bengal in the post-monsoon peak season? *Atmos. Sci. Lett.* **17**, 148–154 (2016).
- Wang, G., Su, J., Ding, Y. & Chen, D. Tropical cyclone genesis over the South China Sea. *J. Mar. Syst.* **68**, 318–326 (2007).
- Yang, H., Jia, X. & Li, C. The tropical Pacific–Indian Ocean temperature anomaly mode and its effect. *Chin. Sci. Bull.* **51**, 2878–2884 (2006).
- Li, C. Y., Li, X., Yang, H., Pan, J. & Li, G. Tropical Pacific–Indian Ocean associated mode and its climatic impacts. *Chin. J. Atmos. Sci.* **42**, 505–523 (2018).
- Li, X. & Li, C. The tropical Pacific–Indian Ocean associated mode simulated by LICOM2.0. *Adv. Atmos. Sci.* **34**, 1426–1436 (2017).
- Girishkumar, M. S., Thanga Prakash, V. P. & Ravichandran, M. Influence of Pacific Decadal Oscillation on the relationship between ENSO and tropical cyclone activity in the Bay of Bengal during October–December. *Clim. Dyn.* **44**, 3469–3479 (2015).
- Li, Z., Xu, Z., Fang, Y. & Li, K. Influence of the Interdecadal Pacific Oscillation on super cyclone activities over the Bay of Bengal during the primary cyclone season. *Atmosphere* **13**, 685 (2022).
- Yang, L. et al. Characteristics of rapidly intensifying tropical cyclones in the South China Sea, 1980–2016. *Adv. Clim. Chang. Res.* **13**, 333–343 (2022).
- Zheng, M. & Wang, C. Interdecadal changes of tropical cyclone intensity in the South China Sea. *Clim. Dyn.* **60**, 409–425 (2023).
- Bhardwaj, P., Singh, O., Pattanaik, D. R. & Klotzbach, P. J. Modulation of Bay of Bengal tropical cyclone activity by the Madden-Julian Oscillation. *Atmos. Res.* **229**, 23–38 (2019).
- Rahul, R., Kuttippurath, J., Chakraborty, A. & Akhila, R. S. The inverse influence of MJO on the cyclogenesis in the North Indian Ocean. *Atmos. Res.* **265**, 105880 (2022).
- Ling, Z., Wang, Y. & Wang, G. Impact of intraseasonal oscillations on the activity of tropical cyclones in summer over the South China Sea. Part I: local tropical cyclones. *J. Clim.* **29**, 855–868 (2016).
- Dao, L. T. & Yu, J. Impacts of Madden-Julian Oscillation on tropical cyclone activity over the South China Sea: Observations versus HiRAM simulations. *Int. J. Climatol.* **41**, 830–845 (2021).
- Zhu, L., Lin, F. & Liang, C. Modulation of tropical cyclone activity over the Northwestern Pacific through the quasi-biweekly oscillation. *J. Trop. Meteorol.* **27**, 125–135 (2021).
- Hu, P., Huangfu, J., Chen, W. & Huang, R. Impacts of early/late South China Sea summer monsoon withdrawal on tropical cyclone genesis over the western North Pacific. *Clim. Dyn.* **55**, 1507–1520 (2020).
- Hersbach, H. et al. The ERA5 global reanalysis. *Q. J. R. Meteorol. Soc.* **146**, 1999–2049 (2020).
- Huang, B. et al. Extended reconstructed sea surface temperature, version 5 (ERSSTv5): upgrades, validations, and intercomparisons. *J. Clim.* **30**, 8179–8205 (2017).
- Rayner, N. et al. Global analyses of sea surface temperature, sea ice, and night marine air temperature since the late nineteenth century. *J. Geophys. Res. Atmos.* **108**, 4407 (2003).
- Hu, C., Zhang, C., Yang, S., Chen, D. & He, S. Perspective on the northwestward shift of autumn tropical cyclogenesis locations over the western North Pacific from shifting ENSO. *Clim. Dyn.* **51**, 2455–2465 (2018).
- Bretherton, C. S., Smith, C. & Wallace, J. M. An intercomparison of methods for finding coupled patterns in climate data. *J. Clim.* **5**, 541–560 (1992).
- Richter, I., Stuecker, M. F., Takahashi, N. & Schneider, N. Disentangling the North Pacific Meridional Mode from tropical Pacific variability. *npj Clim. Atmos. Sci.* **5**, 94 (2022).
- Wu, L. & Wang, B. Assessing impacts of global warming on tropical cyclone tracks. *J. Clim.* **17**, 1686–1698 (2004).

57. Wang, B. & Murakami, H. Dynamic genesis potential index for diagnosing present-day and future global tropical cyclone genesis. *Environ. Res. Lett.* **15**, 114008 (2020).
58. Murakami, H. & Wang, B. Future change of North Atlantic tropical cyclone tracks: projection by a 20-km-mesh global atmospheric model. *J. Clim.* **23**, 2699–2721 (2010).
59. Emanuel, K. & Nolan, D. S. Tropical cyclone activity and the global climate system. In *proceedings of the 26th conference on hurricanes and tropical meteorology* (2004).
60. Hurrell, J. W., Hack, J. J., Shea, D., Caron, J. M. & Rosinski, J. A new sea surface temperature and sea ice boundary dataset for the Community Atmosphere Model. *J. Clim.* **21**, 5145–5153 (2008).

ACKNOWLEDGEMENTS

This work was jointly supported by grants from the National Natural Science Foundation of China (42088101, 41975077), the Innovation Group Project of Southern Marine Science and Engineering Guangdong Laboratory (Zhuhai) (No. 311022001), the Guangdong Province Key Laboratory for Climate Change and Natural Disaster Studies (Grant 2020B1212060025), the National Program on Global Change and Air-Sea Interaction (GASI-IPOVAI-04), and the Zhuhai Joint Innovative Center for Climate, Environment and Ecosystem. This study is also supported by the open fund of State Key Laboratory of Satellite Ocean Environment Dynamics, Second Institute of Oceanography, MNR (No. QNHX2331).

AUTHOR CONTRIBUTIONS

Z.W. and C.H.: Conceptualization, Designation, Writing–review & editing. Z.W.: Data analysis, Visualization, Writing–original draft. C.H. and Z.W.: Numerical Experiments. All authors discussed the results throughout the whole process.

COMPETING INTERESTS

The authors declare no competing interests.

ADDITIONAL INFORMATION

Supplementary information The online version contains supplementary material available at <https://doi.org/10.1038/s41612-023-00506-z>.

Correspondence and requests for materials should be addressed to Chundi Hu.

Reprints and permission information is available at <http://www.nature.com/reprints>

Publisher's note Springer Nature remains neutral with regard to jurisdictional claims in published maps and institutional affiliations.



Open Access This article is licensed under a Creative Commons Attribution 4.0 International License, which permits use, sharing, adaptation, distribution and reproduction in any medium or format, as long as you give appropriate credit to the original author(s) and the source, provide a link to the Creative Commons license, and indicate if changes were made. The images or other third party material in this article are included in the article's Creative Commons license, unless indicated otherwise in a credit line to the material. If material is not included in the article's Creative Commons license and your intended use is not permitted by statutory regulation or exceeds the permitted use, you will need to obtain permission directly from the copyright holder. To view a copy of this license, visit <http://creativecommons.org/licenses/by/4.0/>.

© The Author(s) 2023